5

Enhancement of Wind Energy Penetration Levels using Adaptive Delayed LMF Control Algorithm

This chapter presents the Delayed Least Mean Fourth controlled DSTATCOM based method for enhancing wind energy penetration level in the rural grid by mitigating the PQ disturbances under the MATLAB and experimental environments. Power quality issues associated with variable wind speeds, different grid strength, loads composition, and wind penetration levels have been investigated. Finally, the effectiveness of the proposed algorithm has been compared using algorithms published in the literature.

5.1 INTRODUCTION

Wind Energy (WE) sources, coupled with custom power devices, promise quantum improvement in expense, performance capability, power quality, and reliability. The WE sources have been considered the most leading sources of power generation by 2050 because they help to minimize the capital expenses for the generation of renewable power and meet the load demand in metropolitan and rural areas [Blaabjerg and Ma, 2017]. These growths can pave the way for a modern WE power generation revolution for the rural areas. The rural grid is generally located in remote or hilly areas. Due to the large distances from the central grid, the line's impedance increases and the short circuit ratio decreases. Thus, the grid's strength is degraded and termed the weak grid. Integrating these sources into the rural grid decreases the household's peak load demand and provides more economical energy costs to benefit the consumer. However, this connection is presented multiple challenges to utilities due to the inconsistent wind output, connected loads, interfacing converters, and strength of the AC grid [Brekken and Mohan, 2007]. [Chi *et al.*, 2019], established that the accurate reactive power planning and additional DSTATCOM infrastructure can resolve the said challenges and enable a high WE penetration level. Therefore, an appropriate control algorithm for DSTATCOM is required to adapt to the changes associated with the changes in the system and generate optimum switching signals.

5.2 MERITS OF DELAYED LMF CONTROL ALGORITHM

The conventional Phase Locked Loop (PLL) interfaced vector control scheme [Fan and Miao, 2018] and its modification [Zhang *et al.*, 2020] were developed for enhancing the performance of the DFIG wind energy system. These investigations reported that the PLL would shape the inverter's quadrature-axis output impedance into a negative resistance in the low-frequency band. And this would be responsible for the instability of the inverter under a low SCR of grid [Li *et al.*, 2020b]. Therefore, a proper PLL's bandwidth selection criteria are essential for ensuring the stability in weak grid [Wu *et al.*, 2020]. These conventional controls are also facing the problem of incorrect parameter calculations during any changes in the system, especially varying strength of ac grid [Ali *et al.*, 2018]. Hence, the DC-link voltage of the converter is not maintained within the specified range, and frequency stability is majorly disturbed [Li *et al.*, 2019b]. However, the primary features desired in weak grid control and operation are quick response and adaption of

control algorithms with the changes associated with the dynamics of the converters, loads, strength of grid and WE generation, which are hard to achieve with conventional schemes. Hence, the researchers started to explore the capability of adaptive control algorithms in PQ improvement, which enables high WE penetration levels. Various adaptive control algorithms have been developed in the literature. [Li *et al.*, 2020a] proposed a wide-band harmonic voltage feed-forward control strategy for the mitigation of sub-synchronous resonance (SSR) issue in a grid with SCR of 2. The voltage stability under grid SCR of 2 was maintained using the coordinated control strategy of cascaded H-bridge STATCOM [Peng *et al.*, 2021]. A hybrid generalized integrator scheme has been implemented for compensating the weak grid voltage unbalancing and harmonics [Chishti *et al.*, 2020]. The intelligent heuristic algorithm has been implemented to mitigate harmonics in the utility grid with an SCR of 2 [Zhang *et al.*, 2020]. Still, their performances did not examine under the conditions of various grid strength, wind speeds and non-linear loads, which is essential for the rural grid application. These adaptive algorithms are still in the early phases of development, so understanding the significant benefits of high WE penetration levels and overcoming the challenges associated with a weak grid would lead to its widespread use. However, the proposed adaptive control algorithm ensures reliable operation with maintaining PQ standards due to the attractive features, including simple architecture, simplified calculation, Experimental compatibility, PLL-less structure, adaptiveness, minor steady-state error, and estimation accuracy power.

5.3 SYSTEM CONFIGURATION

The system configuration of the rural grid with high WE penetration is depicted in Fig. 5.1, where the DSTATCOM is employed to inject the required reactive power and improve the PQ for enhancement of WE penetration into the rural grid. The base MVA and base voltage are selected to be 6 MW and 0.415 kV, respectively, for the per-unit (p.u.) calculations. The details of the various parameter used for the system configuration is presented in Table 5.1.

Table 5.1: System parameters.

Parameters	MATALB simulation values	Experimental values
Type-III DFIG	1.5 MW,3 MW,4.5 MW,6 MW	0.400 kW
WE penetration level (30%)	6 MW, 575 V	0.400 kW, 415 V
Wind speed variations	15 m/s and 7.5 m/s	12 m/s and 7.2 m/s
SCR of grid	2.74, 5 and 7	2.74, 5 and 7
X/R ratio of grid	7	7
Step down transformer	0.575 kV / 0.415 kV	-
Linear loads at 0.8-lagging PF (100%)	19.5 MW	1.330 kW
Linear loads at 0.8-lagging PF (60%)	11.7 MW	0.798 kW
Rectifier based NL loads (40%)	7.8 MW	0.532 kW
DSTATCOM	6 MVAr, 680 Vdcd	5 kVAr, 500 Vdcd

5.4 DESIGNING OF DELAYED LMF ALGORITHM

The design considerations of the basic and proposed delayed LMF algorithm is explained in following subsections.

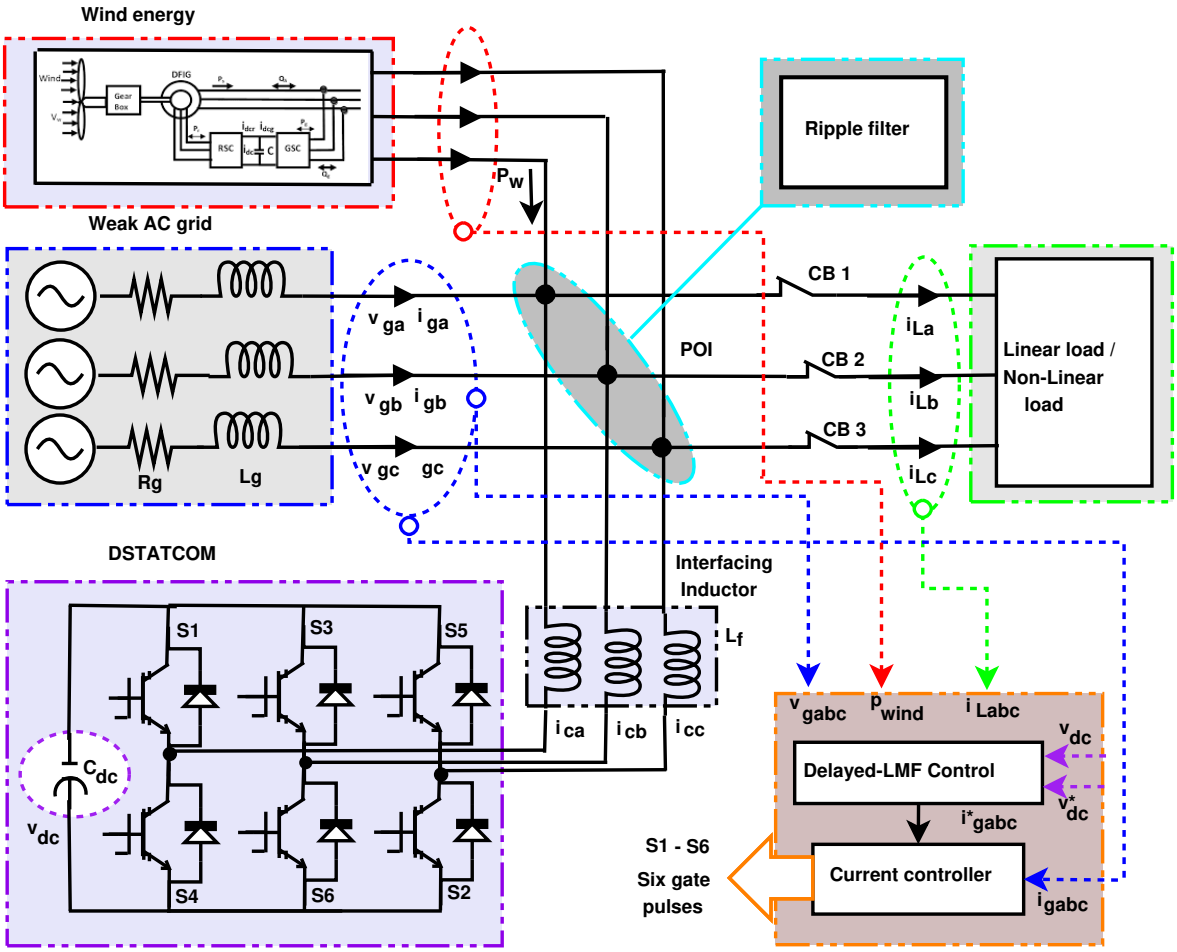

Figure 5.1: The system configuration of the rural grid.

5.4.1 Standard Delayed LMS Algorithm

The following equations describe the delayed-least mean square (DLMS) algorithm:

$$y(n) = X^T(n) \times W(n-1-D_1) \tag{5.1}$$

$$e(n) = d(n) - y(n) \tag{5.2}$$

The DLMS updation equation

$$W(n) = W(n-1-D2) + \tau \times e(n-D_3)X(n-D_4) \tag{5.3}$$

The DLMF updation equation

$$W(n) = W(n-1-D2) + \tau \times e^3(n-D_3)X(n-D_4) \tag{5.4}$$

W(n); the coefficient vector of the filter of order N, X(n):the input vector, d(n);desired signal, y(n);the output signal of the filter. D_1, D_2, D_3, D_4 are four different types of delays and τ is the step size. e and e^3 are the errors of the DLMS and DLMF, respectively. It has been observed from [Long *et al.*, 1989] that, the convergence mainly depends on the selection of the appropriate value of these constants.

5.4.2 Basic Designing of Delayed LMF Algorithm

The delayed least mean square (DLMS) algorithm comes from the adaptive algorithms family, proposed by [Haykin and Widrow, 2003]. The adaptive capability and accurate tracking of

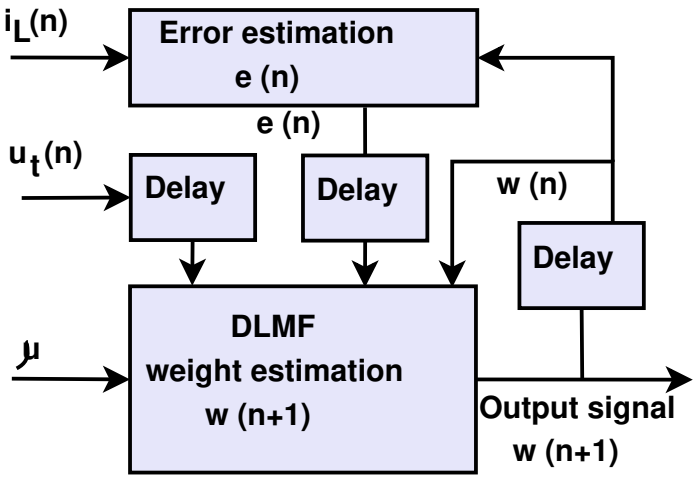

Figure 5.2: Block diagram of weight estimation using the DLMF algorithm.

signals considering changes associated with the system using delayed constant are the significant features of this algorithm. This algorithm updates the old data based on the system changes' new information, which helps estimate active and reactive weight components. The delay constant plays an essential role during data updation by providing preceding cycle data information. The price to pay for this is an increase in computational time. Motivated by these aspects, a concept is proposed in [Huu Tue Huynh *et al.*, 1997] for fast convergence of DLMS. The performance of DLMS is superior to the LMS using the adaption delay of D_1, D_2, D_3, D_4 as 5, 0, 1, 1, respectively, along with the step size of 0.018. The designing of the proposed algorithm considers the outcomes of this paper by taking adaptive delay constant and step size. After designing the DLMS algorithm, it has been converted into the DLMF algorithm using the LMF algorithm [Gui *et al.*, 2014] for solving complexity and stability issues.

$$w(n) = w(n-1-D_2) + \tau \times x(n-D_4) \times e^3(n-D_3) \tag{5.5}$$

$$y(n) = x(n) \times w(n-1-D_1) \tag{5.6}$$

$$e^3(n) = d(n) - y(n) \tag{5.7}$$

Where, weight vector $w(n)$, input vector $x(n)$, desired output $d(n)$, filter output $y(n)$, adaption delay (D) and step size (τ).

5.4.3 Proposed Delayed LMF Control Algorithm

The proposed algorithm is simulated in such a way that the system signals continuously update active (Wp) and reactive weight (Wq) components considering appropriate delays. These delay constants help to track accurate signals using previous cycle data details. Thereby manages the required reactive power at PCC, and harmonics in the system becomes mitigated shown in Fig. 5.2. The block diagram of weight estimation using the ADALINE-LMS algorithm is as presented in Fig. 5.2. It can be observed that weights are estimated and updated after every iteration using appropriate delay. The updated weights are used to calculate reference grid currents to switch the DSTATCOM as shown in Fig. 5.3. The processes involved for the design and implementation of the proposed DLMF algorithm is similar to the least mean fourth based control algorithm [Agarwal *et al.*, 2016b].

1. **Estimation of Voltage Unit Templates** The peak amplitude of terminal voltage (v_t) is

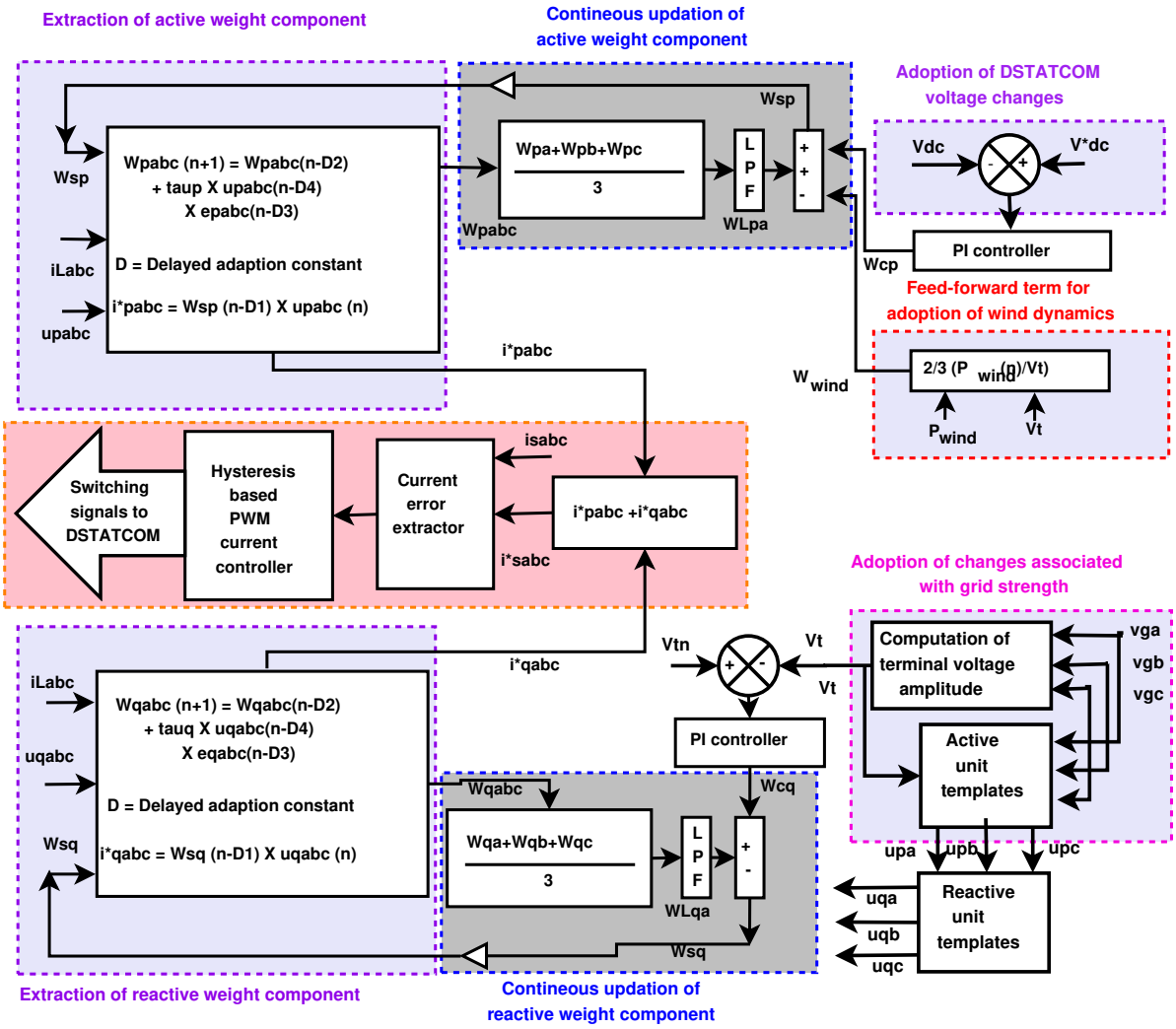

Figure 5.3: Block diagram of proposed adaptive DLMF control algorithm.

calculated using the three-phase grid voltage.

$$v_t = \sqrt{2/3(v_{sa}^2 + v_{sb}^2 + v_{sc}^2)} \tag{5.8}$$

In-phase (active) and quadrature (reactive) unit templates are,

$$\left\{ \begin{array}{c} u_{pabc} = v_{sabc}/v_t \\ u_{qa} = -u_{pb}/\sqrt{3} + u_{pc}/\sqrt{3} \\ u_{qb} = \sqrt{3}u_{pa}/2 + (u_{pb} - u_{pc})/2\sqrt{3} \\ u_{qc} = -\sqrt{3}u_{pa}/2 + (u_{pb} - u_{pc})/2\sqrt{3} \end{array} \right\} \tag{5.9}$$

Sensed three-phase weak grid voltages are divided by the v_t to calculate active unit templates (u_{pabc}). Initially, these unit voltage templates are not unity due to low SCR of the grid. However, these voltage templates required to keep unity for maintaining voltage stability during high WE penetration[Mohod and Aware, 2010].

2. **Estimation of Loss Components** The PI voltage regulator is used to estimate the active and reactive loss components. The accurate estimation of DC link voltage is essential for minimizing the voltage fluctuations during the high wind power penetration at PCC. In this regard, the PI regulator has tuned with the optimum value of proportional $K_{pd} = 0.30$ and integral $K_{id} = 0.30$ gains. This regulator generates an active loss component (W_{cp}) for

maintaining dc-bus voltage. Further, the obtained loss component is utilized to control the dc-bus voltage at n^{th} sampling instant,

$$W_{cp}(n+1) = W_{cp}(n) + k_{pd}(v_{de}(n+1) - v_{de}(n)) + k_{id}v_{de}(n+1) \tag{5.10}$$

where, $W_{cp}(n+1)$ and $v_{de}(n+1)$ are the updated active loss component and dc voltage error and the present value of this dc voltage error is obtained using $v_{de}(n) = v^*_{dc}(n) - v_{dc}(n)$. where, (v^*_{dcd}) is the reference dc link voltage obtained from $(v^*_{dcd} = 2\sqrt{2} \times v_{LL}/\sqrt{3} \times m)$. v_{LL} is represent voltage (line to line) at PCC and m is the modulation index.

Similarly, reactive loss component (W_{cq}) is estimated as,

$$W_{cq}(n+1) = W_{cq}(n) + k_{pq}(v_{te}(n+1) - v_{te}(n)) + k_{iq}v_{te}(n+1) \tag{5.11}$$

where, $W_{cq}(n+1)$ and $v_{te}(n+1)$ are updated reactive loss component and voltage error. However the present value of this voltage error is obtained using $v_{te}(n) = v_{tn}(n) - v_t(n)$.

The stability analysis of the proposed control algorithm is carried out for dc bus control of DSTATCOM. The transfer function T_S(s) is given as,

$$T_s(s) = T_p(s) \times T_c(s) = [(1/sc_{dc}) \times (k_p + (k_i/s))] \tag{5.12}$$

Where, T_p(s) and T_c(s) are the transfer function of plant and PI voltage regulator. The Bode stability diagram is plotted with the help of system parameters. It is perceived from the Bode stability plot that, the phase margin is in the stable region. Thus the system is in the stable condition illustrated in Fig 5.4.

3. **Extraction of Weight and Error Components of Load Current** The active and reactive weight components of load currents are extracted using the concept of adaption delay of DLMF.

$$w_{pabc}(n+1) = w_{pabc}(n - D_2) + \tau_p \times u_{pabc}(n - D_4) \times e^3_{pabc}(n - D_3) \tag{5.13}$$

$$w_{qabc}(n+1) = w_{qabc}(n - D_2) + \tau_q \times u_{qabc}(n - D_4) \times e^3_{qabc}(n - D_3) \tag{5.14}$$

where, $W_{pabc}(n+1)$ are updated three-phase active weight components of load current (i_{Labc}). The active and reactive error components are represented as $(e^3_{pabc}(n)$ and $(e^3_{qabc}(n))$ respectively. Also, the accuracy of estimation and the convergence are based on the value of step size constant (τ_p and τ_q) and it is selected as 0.018.

$$e^3_{pabc}(n) = i_{Labc}(n) - u_{pabc}(n) \times w_{pabc}(n) \tag{5.15}$$

$$e^3_{qabc}(n) = i_{Labc}(n) - u_{qabc}(n) \times w_{qabc}(n) \tag{5.16}$$

where, $i_{Labc}(n)$ load currents, $w_{pabc}(n)$ and $w_{qabc}(n)$ are the weights of active and reactive reference component. The $u_{pabc}(n)$ and $u_{qabc}(n)$ are active and reactive unit templates of weak ac system.

4. **Wind Feed-Forward Term** The wind-feed-forward term (W_{wind}) is implemented in the algorithm to adapt the changes in wind output power. It is calculated using current output power (P_{wind}) of WE source,

$$W_{wind}(n) = 2P_{wind}(n)/3v_t \tag{5.17}$$

5. **Estimation of Total Active and Reactive Weight Components** However, to minimize the effect of load current during high WE penetration weights are averaged. The fundamental active weight component of reference grid currents is written as,

$$W_{Lpa}(n) = \{W_{pa}(n) + W_{pb}(n) + W_{pc}(n)\}/3 \tag{5.18}$$

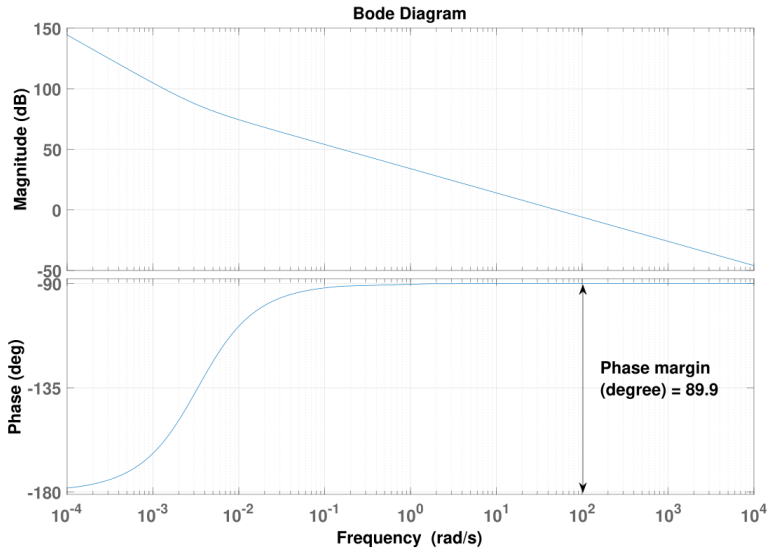

Figure 5.4: Bode stability diagram of DLMF control using controller inputs.

Where, $W_{pa}(n)$, $W_{pb}(n)$ and $W_{pc}(n)$ are weight components of load current signals corresponding to all phases. For the accurate adoption of system dynamics in the algorithm, the total weight component should update with the changes associated with the DC-link voltage of the DSTATCOM. Thus, the output of PI regulator (W_{cp}) should be added to the averaged weight $W_p(n)$ and subtracting the wind feed-forward weight ($W_{wind}(n)$) to updated total weight component $W_{sp}(n)$.

$$W_{sp}(n) = W_p(n) + I_p(n) - W_{wind}(n) \tag{5.19}$$

Similarly, the total reactive weight component (W_{sq}) is calculated by subtracting the average reactive weight component (W_{Lqa}) to the ac loss component (W_{cq}). However, W_{Lqa} is computes using ($W_{Lqa} = (W_{qa} + W_{qb} + W_{qc})/3$) relation.

$$W_{sq} = W_{cq} - W_{Lqa} \tag{5.20}$$

6. **Generation of Reference Grid Currents** The active reference signal (i^*_{pabc}) is estimated using total active weight component (W_{sp}) and unit templates. Similarly, the reactive reference signals (i^*_{qabc}) are estimated using reactive weight component (W_{sq}) and unit templates.

$$i^*_{pabc} = W_{sp}(n - D_1) \times u_{pabc}(n) \tag{5.21}$$

$$i^*_{qabc} = W_{sq}(n - D_1) \times u_{qabc}(n) \tag{5.22}$$

Thus, three phase reference grid current signals are generated by combining (i^*_{pabc}) and (i^*_{qabc}) signals,

$$i^*_{sabc} = i^*_{pabc} + i^*_{qabc} \tag{5.23}$$

7. **Generation of Switching Signals** The three-phase switching signals are generated using weak grid currents (i^*_{sabc}) and actual weak grid currents (i_{sabc}) with current band (cb=0.1) of hysteresis current controller by following logic: If (i_{sabc}) > ($i^*_{sabc} + cb$), the upper switch is ON and lower switch is OFF. If (i_{sabc}) < ($i^*_{sabc} - cb$), the lower switch is ON and upper switch is OFF.

5.5 SIMULATION RESULTS AND DISCUSSIONS

The performance of the proposed methodology has been demonstrated by simulating unbalance with various strengths of the grid, different compositions of the loads and various penetration levels of WE. The description of the case studies is presented in Table 5.2.

Table 5.2: Parameter variations for various case studies.

S.No.	Parameters	Parameter Variations	
		Simulation	Experimental
1	SCR	2.74, 5 and 7	2.74, 5 and 7
2	Load-1	100% linear 0.8 lag-PF load	100% linear 0.8 lag-PF load
3	Load-2	40% NL load + 60% linear load	40% NL load + 60% linear load
4	WE Penetration levels	10%, 18%, 25% and 30%	10%, 18%, 25% and 30%
5	Wind speed variation	Rated 15m/s to Mini. 7.5 m/s	Rated 12 m/s to Mini. 7.2 m/s
6	Synchronization point	at 1 second	at 1 second

5.5.1 Case-1: Enhancement of WE Penetration Levels

The penetration levels are enhanced from 10% to 30% into the grid of SCR 2.74 with 100% linear load. Figure Fig.5.5 presents the 30 % WE penetration level with its voltage. It can be

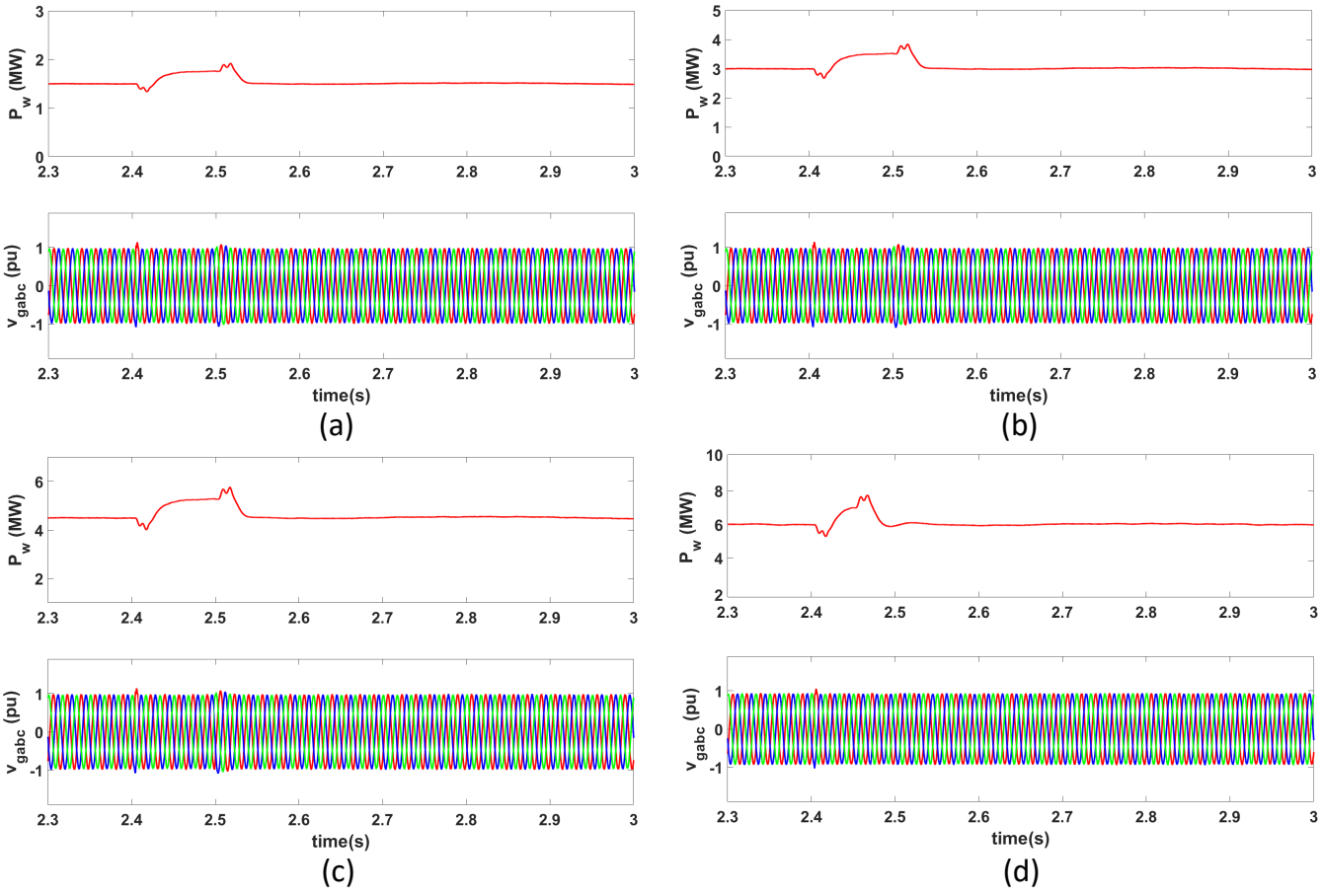

Figure 5.5: WE penetration levels with 100% linear load (a) 10%, (b) 18%, (c) 25%, (d) 30%.

Table 5.3: Enhancement of WE penetration levels (Simulation).

Penetration levels (↓)	Loads (→)	Load-1		
	SCR (→)	2.74	5	7
Simulation analysis				
10%	V_{gTHD}	2.30	2.25	2.23
	i_{gTHD}	0.87	0.81	0.77
	PF_g	1	1	1
	P_w (MW)	1.5	1.5	1.5
	Q_d (MVAr)	0.26	0.25	0.25
	V_g (Volt)	418	416	416
18%	V_{gTHD}	2.61	2.50	2.48
	i_{gTHD}	1.11	1.0	1.0
	PF_g	1	1	1
	P_w (MW)	3	3	3
	Q_d (MVAr)	0.33	0.30	0.30
	V_g (Volt)	418	416	416
25%	V_{gTHD}	2.83	2.80	2.77
	i_{gTHD}	1.31	1.29	1.26
	PF_g	0.98	0.98	0.98
	P_w (MW)	4.5	4.5	4.5
	Q_d (MVAr)	0.40	0.38	0.38
	V_g (Volt)	418	416	416
30%	V_{gTHD}	3.21	3.13	3.11
	i_{gTHD}	1.57	1.44	1.41
	i_{wTHD}	1.71	1.68	1.65
	PF_g	0.98	0.98	0.98
	P_w (MW)	6	6	6
	Q_d (MVAr)	0.42	0.40	0.40
	V_g (Volt)	418	416	416

found that the power quality of the system in terms of voltage is maintained within the stability range (*i.e.* $\pm$ 10%) up to 30 % WE penetration level. Also, the active power of WE sources is tracked with more than 99% accuracy up to 30% WE penetration level. The simulation results are shown in Table 5.3. It is found that increments in the penetration level up to 30% harmonic levels also increase in the system. These harmonic levels are well maintained under the international PQ standards. The power factor, the magnitude of voltage and harmonic levels of voltage and current of the grid are observed to meet PQ standards with increments in the penetration level.

5.5.2 Case-2: Performance with NL Load at Rated Wind Speed

Figure 5.6 presents the various waveforms of the proposed method for mitigating the PQ in a grid with an SCR of 2.74. This case study considers the load combination 40% NL load + 60% linear load and wind penetration level 30%. An unbalance simulated from 2.4 to 2.45-second by disconnecting phase-a of load and connecting it back. Figure 5.6 (a) illustrate the recovery stage (2.44 to 2.475-second). The rapid compensating current (i_{cabc}) is injected by the DSTATCOM to maintain grid voltage and to compensate for unbalance in grid currents during the unbalancing. It can be perceived that the grid voltage (v_{gabc}) and current (i_{gabc}) are continuously balanced and sinusoidal. The total recovery time from the unbalance stage to the balance stage is found to be 0.015 sec with an improved power factor (PF_g), which shows the adaptive capability of the

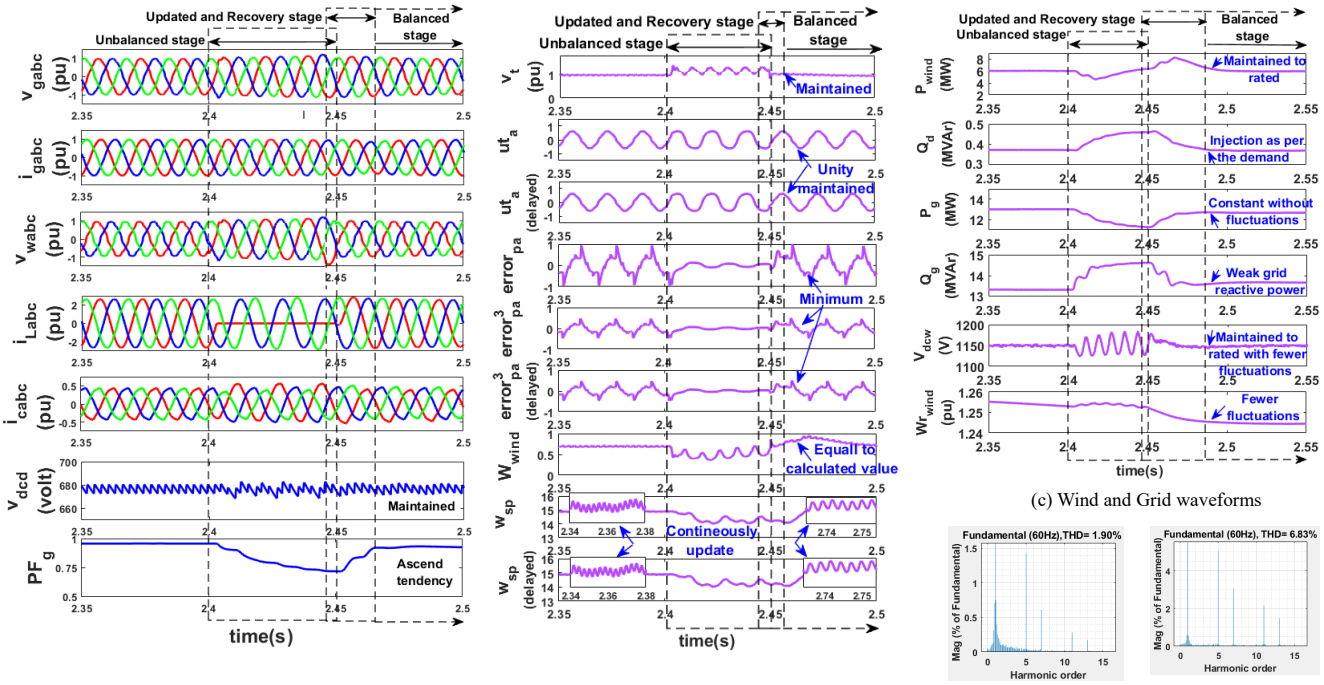

(a) System waveforms (b) Intermediate signals (c) Wind and Grid waveforms (d) THD Ig (d) THD Vg

Figure 5.6: Performance of proposed method with NL load at rated wind speed.

delayed-LMF control algorithm. Meanwhile, the DC-link voltage of the DSTATCOM (v_{dcd}) is maintained to reference value with fewer fluctuations.

The intermediate signals computed in DLMF is depicted in Fig. 5.6 (b). At 2.4-second DSTATCOM provides rapid compensating current (i_{ca}) to stabilize the terminal voltage (V_t) within voltage stability range, ±10%. The voltage unit templates (ut_a) and delayed unit templates ($ut_{a(delayed)}$) of grid are kept unity. The errors ($error^3_{pa}, error^3_{pa(delayed)}$) in current components are found to be minimum. The updated total weight component (w_{sp}) and delayed updated total weight component ($w_{sp(delayed)}$) are getting continuously update. The calculate and simulated wind feed-forward term is found to be ≈0.65.

The DSTATCOM is inject up to 0.45 MVAr reactive power to maintain the rated wind active-power ($P_w = 6$ MW) is depicted in Fig. 5.6 (c). The reactive-power requirement of the weak grid (Q_g) is increased during load unbalancing is effectively compensated by the proposed method. The wind side converter dc-link voltage (V_{dcw}) is maintained at 1150 V. The wind rotor oscillations (Wr_{wind}) are found to be practically damped. Fig. 5.6 (d-f) illustrates the harmonics in the grid current, grid voltage and wind currents are found 1.90%, 6.83% and 3.04%, respectively.

5.5.3 Case-3: Performance with NL Load at Minimum Wind Speed

This case study aims to address PQ issues at changes associated with wind-speed (W_{speed}) variations. The W_{speed} is decreased from rated speed 15 m/s to minimum wind speed 7.5 m/s at the time 2.5-second in the presence of NL load (25% NL + 75% linear load) for an SCR of 2.74, as illustrated in Fig 5.7. The grid voltage (v_{ga}), non-linear load current (i_{la}), voltage unit templates (ut_a), error ($error_{pa}$) signals and terminal voltage (v_t) are found to be stable. The wind side converter (v_{dcw}) and DSTATCOM (v_{dcd}) dc-link voltages are maintained to reference value with fewer fluctuations due to controlled action of DLMF algorithm. However, the active output power of wind (P_w), reactive power (Q_d) of DSTATCOM and grid current (i_{ga}) are decreased with

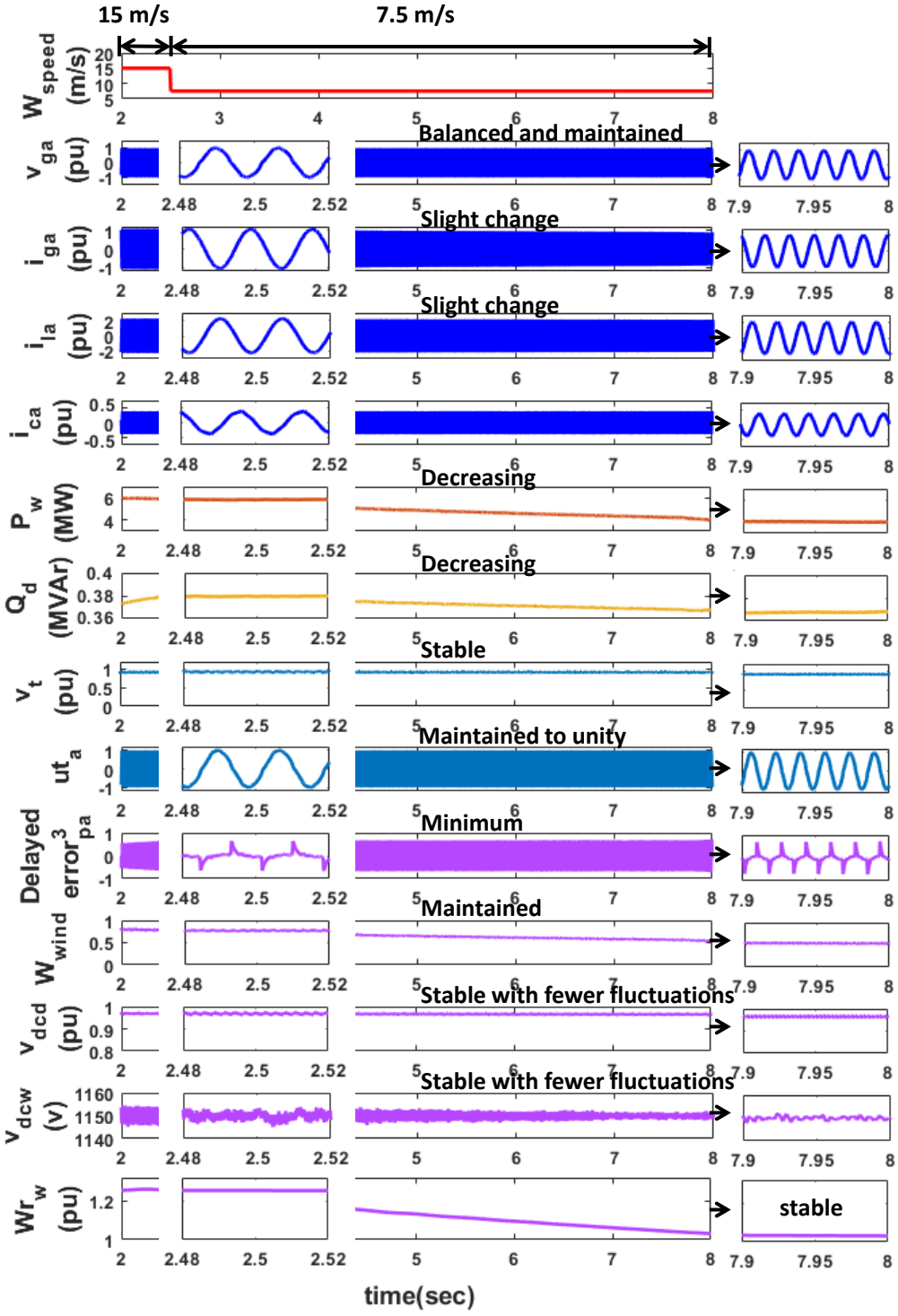

Figure 5.7: Performance of proposed method with NL load at minimum wind speed.

the wind rotor speed (Wr_w). The harmonic levels observed in the grid current and voltage are 2.18% and 4.18% respectively.

5.5.4 Case-4: Effect of Variation in Grid SCR

The proposed algorithm is examined for power quality studies by varying the SCR from 2.74 to 7 with different compositions of unbalanced loads. The power quality analysis of simulation

Table 5.4: Performance under variation in grid SCR (Simulation).

Penetration	Loads (→)	Load-1			Load-2		
levels (↓)	SCR (→)	2.74	5	7	2.74	5	7
Simulation analysis							
10%	V_{gTHD}	2.30	2.25	2.23	6.05	5.97	5.93
	i_{gTHD}	0.87	0.81	0.77	1.30	1.23	1.20
	PF_g	1	1	1	0.99	0.99	0.99
	P_w (MW)	1.5	1.5	1.5	1.5	1.5	1.5
	Q_d (MVAr)	0.26	0.25	0.25	0.30	0.29	0.29
	V_g (Volt)	418	416	416	420	418	417
18%	V_{gTHD}	2.61	2.50	2.48	6.39	6.31	6.29
	i_{gTHD}	1.11	1.0	1.0	1.54	1.46	1.43
	PF_g	1	1	1	0.99	0.99	0.99
	P_w (MW)	3	3	3	3	3	3
	Q_d (MVAr)	0.33	0.30	0.30	0.36	0.34	0.33
	V_g (Volt)	418	416	416	420	418	417
25%	V_{gTHD}	2.83	2.80	2.77	6.60	6.53	6.45
	i_{gTHD}	1.31	1.29	1.26	1.73	1.65	1.61
	PF_g	0.98	0.98	0.98	0.98	0.98	0.98
	P_w (MW)	4.5	4.5	4.5	4.5	4.5	4.5
	Q_d (MVAr)	0.40	0.38	0.38	0.44	0.42	0.42
	V_g (Volt)	418	416	416	420	418	417
30%	V_{gTHD}	3.21	3.13	3.11	6.83	6.72	6.67
	i_{gTHD}	1.57	1.44	1.41	1.90	1.83	1.79
	i_{wTHD}	1.71	1.68	1.65	3.04	2.83	2.79
	PF_g	0.98	0.98	0.98	0.98	0.98	0.98
	P_w (MW)	6	6	6	6	6	6
	Q_d (MVAr)	0.42	0.40	0.40	0.49	0.45	0.44
	V_g (Volt)	418	416	416	420	418	417

studies are present in Table 5.4. The variations in the SCR values from 2.74 to 7 illustrated that slight changes are observed in the second and third decimal of harmonics values. Thus, changes in the SCR of the grid have a negligible effect on the system's performance.

This can also be verified through the stability analysis of the system is carried out for various strengths of the grid using the Bode stability plot. The transfer function $T_g(s)$ for various short circuit ratios of the grid using grid impedance and controller input gains is written as:

$$T_g(s) = T_p(s) \times T_c(s) = \left[\frac{1}{sZ_g} \times (k_p + \frac{k_i}{s})\right] \tag{5.24}$$

T_p(s); Plant transfer function, T_c(s); PI transfer function and Z_g: grid impedance of different SCRs. Fig. 5.8 shows that the stability of the system is degraded with a grid SCR of 1 due to large impedance, and performance is observed as unsatisfactory. The phase margin of grid impedances of SCR-2.74 and SCR-7 are located in the stable region, indicating that the SCR of 2.74 and beyond the system is stable.

5.5.5 Case-5: Synchronization of DFIG with Rural Grid

The waveforms obtained using the DLMF algorithm for soft synchronization of DFIG into the weak grid (SCR=2.74) at 30% WE penetration are similar to those obtained using the

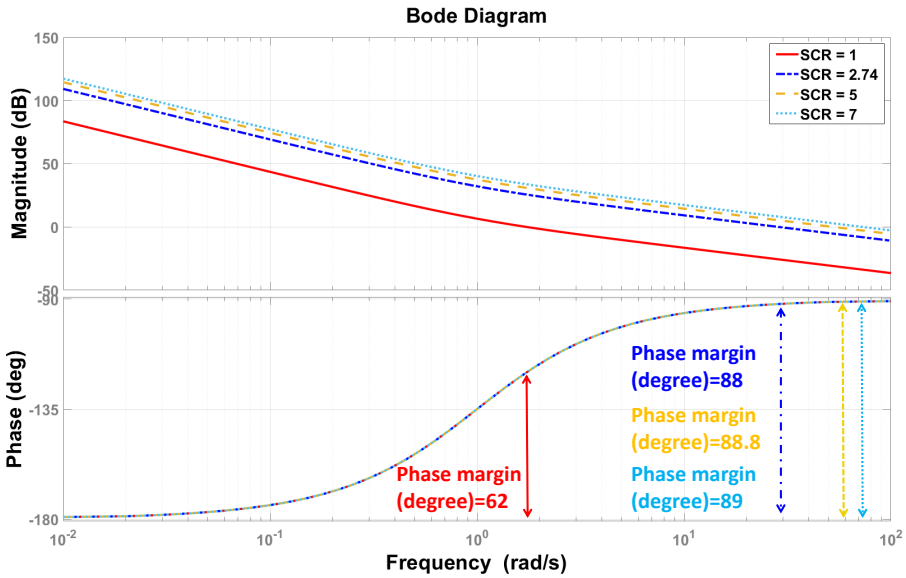

Figure 5.8: Bode stability plot for various grid SCR using grid impedance and controller inputs.

ADALINE-LMS. The WE source and DSTATCOM are connected at 1-second and found that <0.9-s is needed for maintaining soft synchronization. Table 5.7 shows the PQ analysis under the synchronization of DFIG with the rural grid. The observed weak grid, transient (transition) and steady-state (stable) stages voltage and current harmonics are 12.67%, 11.9%, 7.2% and 6.95%, 3.94%, 1.07%, respectively.

5.6 EXPERIMENTAL RESULTS AND DISCUSSIONS

The experimental prototype is depicted in Fig 5.9. The developed prototype consists of SEMIKRON makes VSC based DSTATCOM, and Lucas-Nulle makes a DFIG based WE emulator. The grid currents and voltage signals along with the dc-link voltage of DSTATCOM are sensed using Hall effect based TI-TMCS1100 sensors. The execution of the control algorithm is carried out on DSP (dSPACE-1104). Switching signals are amplified using the buffer-circuit (Microchip-TC427). Tektronix DPO4104B and YOKOGAWA-WT3000 are used to record the waveforms and PQ, respectively. The detailed specifications of the system used for Experimental validation are presented in Table 5.2.

5.6.1 Case-1: Enhancement of WE Penetration Levels

The penetration levels are enhanced from 10% to 30% into the grid of SCR 2.74 with 100% linear load. Figure 5.10 presents the 30 % WE penetration level with its voltage. It can be found that the power quality of the system in terms of voltage is maintained within the stability range ($i.e. \pm 10\%$) up to 30% WE penetration level. Also, the active power of WE sources is tracked with more than 99% accuracy up to 30% WE penetration level. The experimental results are shown in Table 5.5. It is found that increments in the penetration level up to 30% harmonic levels also increase in the system. These harmonic levels are well maintained under the international PQ standards. The power factor, the magnitude of voltage and harmonic levels of voltage and current of the grid are observed to meet PQ standards with increments in the penetration level.

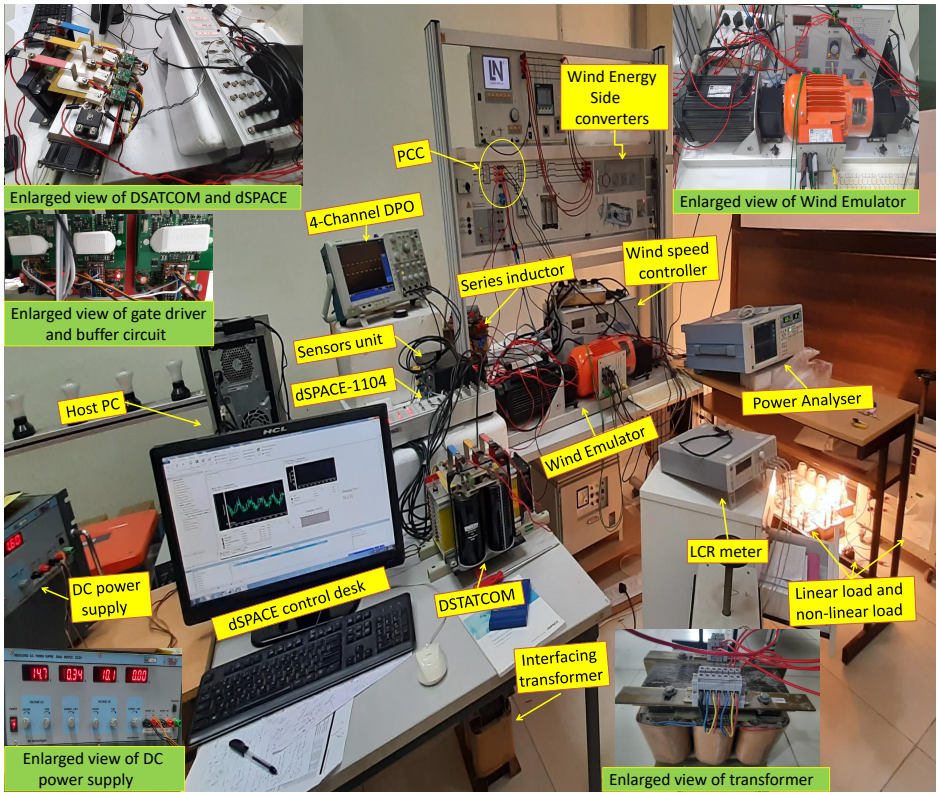

Figure 5.9: Laboratory-based experimental prototype.

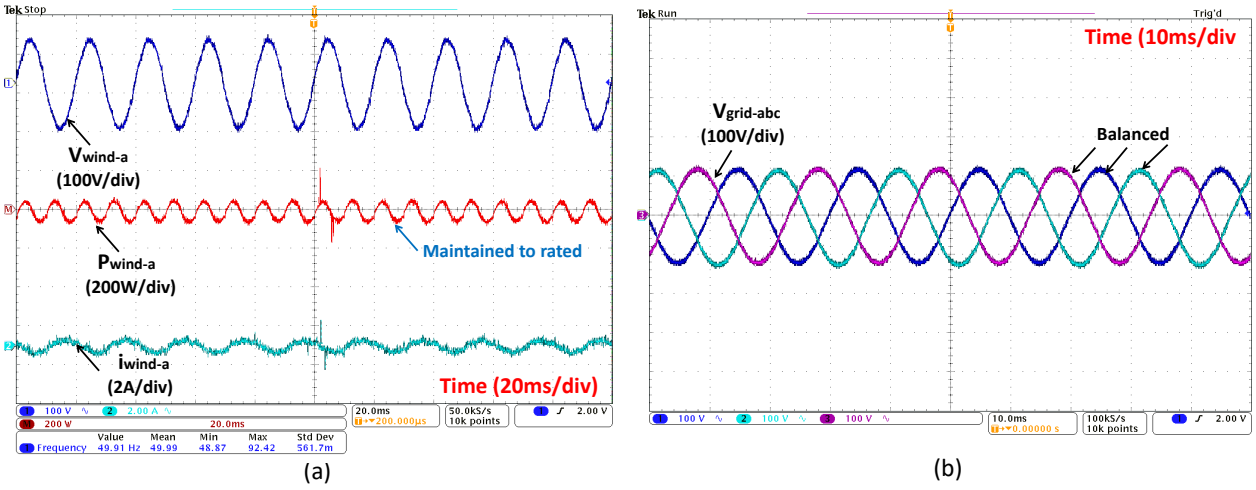

Figure 5.10: WE penetration level with 100% linear load (a) Active power, (b) Grid voltage.

5.6.2 Case-2: Performance with NL Load at Rated Wind Speed

The performance of the system with NL at 30% WE Penetration is illustrated in Fig 5.11 (a). The grid voltage (V_{grid-a}) and current (i_{grid-a}) are observed balanced. The DSTATCOM inject the compensating current (i_{C-a}) to maintain weak grid voltage in the presence of balanced non-linear load (i_{Load-a}).

Fig 5.11 (b) shows the compensating current (i_{C-a}) is being inject by the DSTATCOM to

Table 5.5: Enhancement of WE penetration levels (Experimental).

Penetration levels (↓)	Loads (→)	Load-1		
	SCR (→)	2.74	5	7
Experimental analysis				
10%	V_{gTHD}	2.75	2.71	2.67
	i_{gTHD}	1.0	0.95	0.91
	PF_g	0.98	0.98	0.98
	P_w (kW)	0.279	0.279	0.279
	Q_d (kVAr)	0.0185	0.0146	0.0123
	V_g (Volt)	418	416	416
18%	V_{gTHD}	3.09	2.97	2.92
	i_{gTHD}	1.30	1.24	1.21
	PF_g	0.98	0.98	0.98
	P_w (kW)	0.279	0.279	0.279
	Q_d (kVAr)	0.0234	0.0195	0.0172
	V_g (Volt)	418	416	416
25%	V_{gTHD}	3.26	3.21	3.19
	i_{gTHD}	1.79	1.67	1.67
	PF_g	0.98	0.98	0.98
	P_w (kW)	0.279	0.279	0.279
	Q_d (kVAr)	0.0321	0.0282	0.0259
	V_g (Volt)	416	415	415
30%	V_{gTHD}	3.49	3.41	3.39
	i_{gTHD}	1.97	1.89	1.83
	i_{wTHD}	1.87	1.82	1.78
	PF_g	0.98	0.98	0.98
	P_w (kW)	0.279	0.279	0.279
	Q_d (kVAr)	0.0469	0.0430	0.0407
	V_g (Volt)	418	416	416

maintain grid voltage (v_{grid-a}) and to compensate the unbalance. The steady-state error in the amplitudes of grid current is found to be 0.013 A. During the load unbalance, the compensating current is observed non-sinusoidal due to the harmonics present in the wind current. However, small fluctuations are noted due to the sudden switching of the loads. The DC-link voltage (v_{dcd}) of the DSTATCOM is maintained to reference value. The three-phase grid voltage ($v_{grid-abc}$) and currents ($i_{grid-abc}$) are seen balanced and sinusoidal in Fig 5.11 (c)-(d).

The intermediate signals computed in DLMF control is as depicted in Fig 5.12 (a)-(d). The DC-link voltage of the DSTATCOM and unit voltage template (u_{t-a}) is maintained at their reference value. The calculated, simulated and Experimental wind feed-forward values are found to be similar ($W_{wind} \sim 0.65A$), which illustrated the efficacy of the proposed method.

Fig. 5.12 (c) shows the updated total weight (W_{sp-a}) and delayed updated total weight ($delayed - W_{sp-a}$) components are continuously updating based on the system data. The unit voltage template (u_{t-a}) and delayed unit voltage template ($delayed - u_{t-a}$) are maintained unity. Fig. 5.12 (d) illustrates the least mean square (LMS)($error_a$) and LMF ($error_a^3$) errors have high distortion in the signal compared to DLMF ($delayed - error_a^3$) error. These low distortion into the current error components also shows the accurate tracking performance of the DFMF control algorithm.

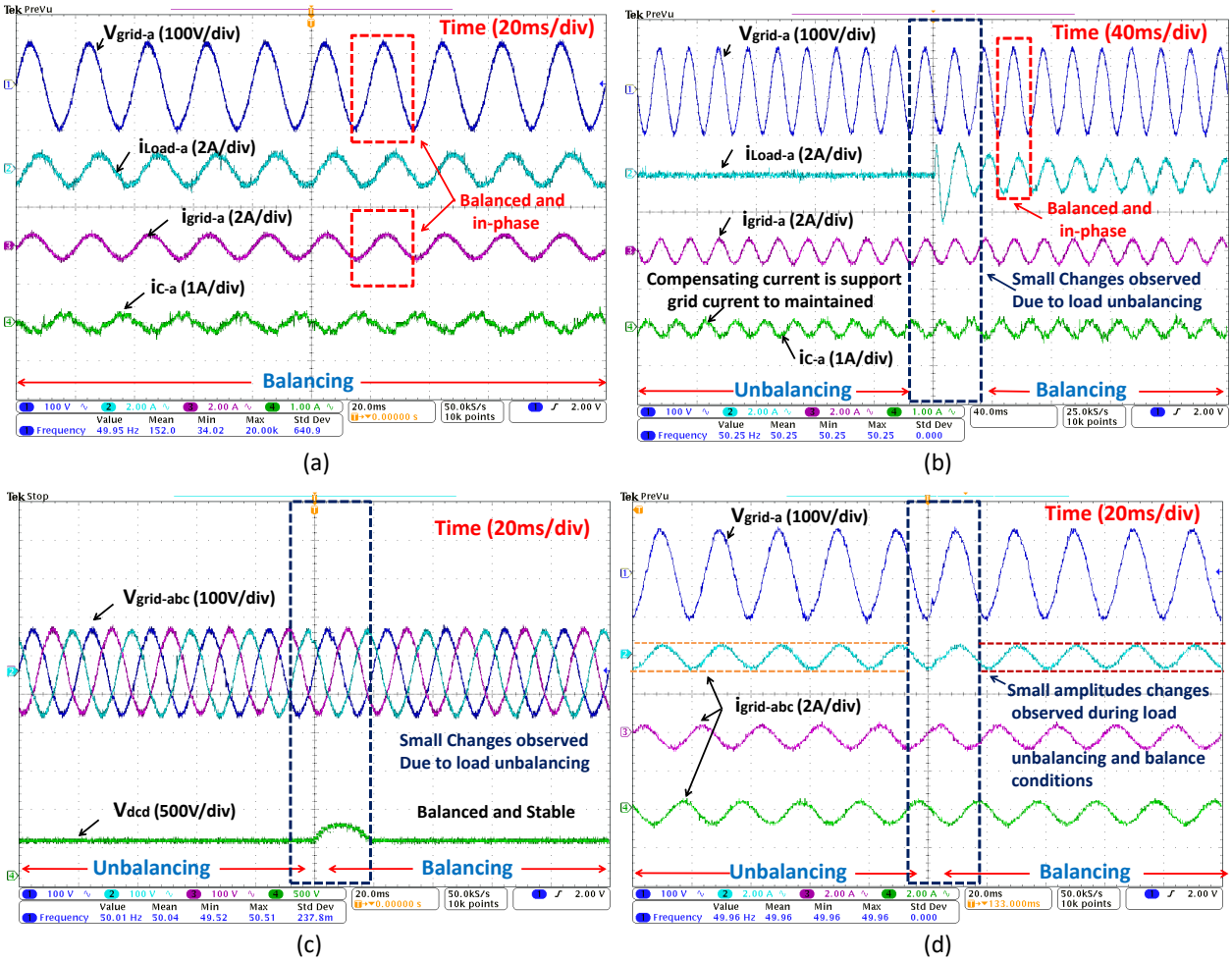

Figure 5.11: Performance of proposed method at rated wind speed. (a) With balanced NL load. (b),(c),(d) With unbalanced NL load.

5.6.3 Case-3: Performance with NL Load at Minimum Wind Speed

Similar case studies are performed with the minimum wind speed (7.2 m/s) presented in Fig 5.13 (a-b). It can be observed from the results that grid voltage (V_{grid-a}) and wind voltage (V_{wind-a}) are maintained within the voltage stability range. The dc-link voltage (v_{dcd}) of the DSTATCOM is also maintained to reference value. However, the amplitudes of the grid current (i_{grid-a}) and wind current (i_{wind-a}) signals are found less due to the reduction in the wind speed. The harmonic levels of voltage and current are found to be 5.6% and 1.82%, respectively.

5.6.4 Case-4: Effect of Variation in Grid SCR

The proposed algorithm is examined for power quality studies by varying the SCR from 2.74 to 7 with different compositions of unbalanced loads. The power quality analysis of experimental studies is present in Table 5.6. The variations in the SCR values from 2.74 to 7 illustrated that slight changes are observed in the second and third decimal of harmonics values. Thus, changes in the SCR of the grid have a negligible effect on the system's performance.

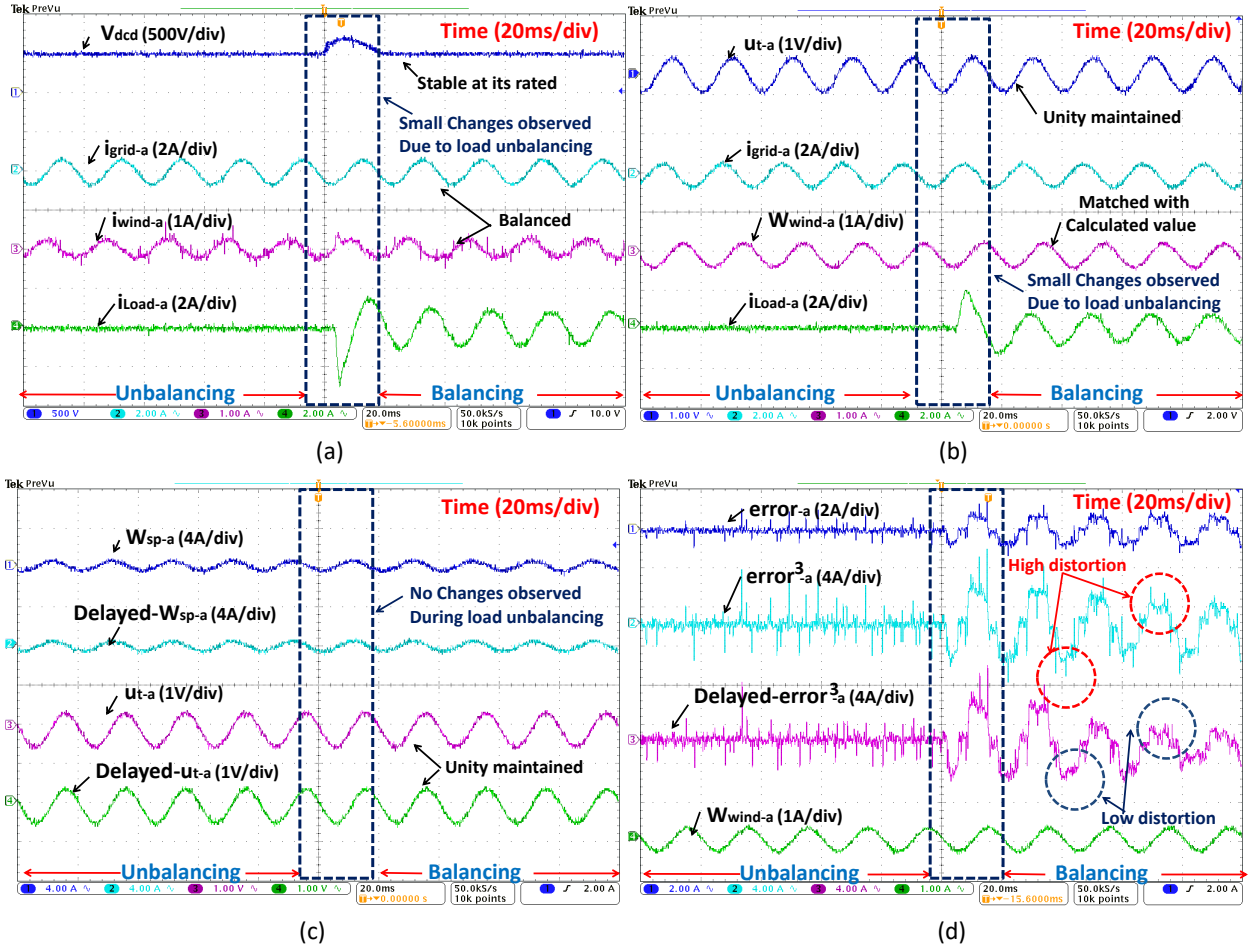

Figure 5.12: Performance of the proposed method at rated wind speed. (a),(b),(c),(d) With unbalanced three-phase NL load.

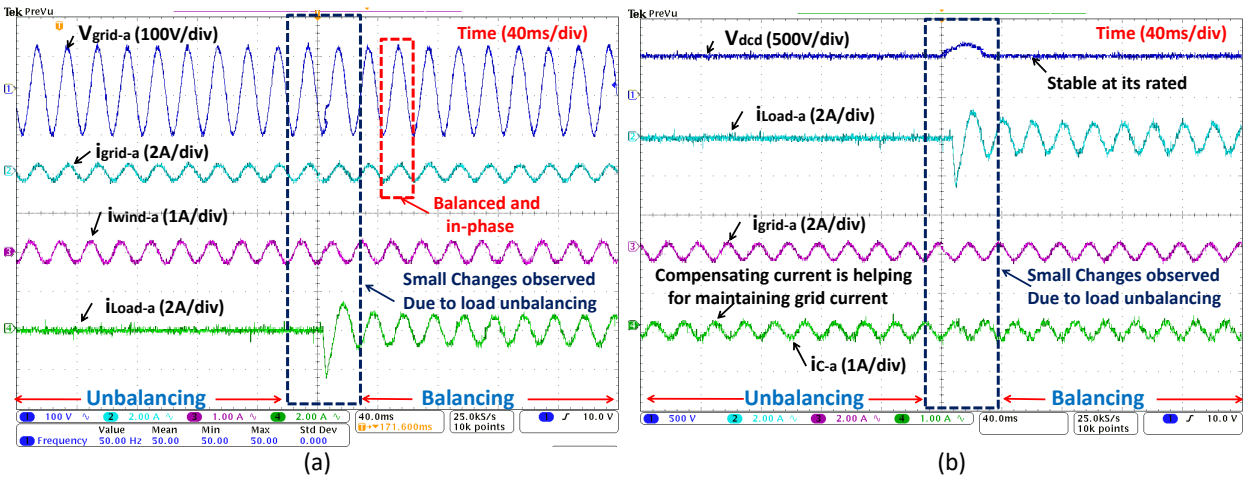

Figure 5.13: Performance of proposed method at minimum wind speed. (a),(b) With unbalanced NL load.

5.6.5 Case-5: Synchronization of DFIG with Rural Grid

The waveforms obtained using the DLMF algorithm for soft synchronization of DFIG into the weak grid (SCR=2.74) at 30% WE penetration are similar to those obtained using the

Table 5.6: Performance under variation in grid SCR (Experimental).

Penetration levels (↓)	Loads (→)	Load-1			Load-2		
	SCR (→)	2.74	5	7	2.74	5	7
		Experimental analysis					
10%	V_{gTHD}	2.75	2.71	2.67	6.53	6.49	6.46
	i_{gTHD}	1.0	0.95	0.91	1.51	1.47	1.43
	PF_g	0.98	0.98	0.98	0.98	0.98	0.98
	P_w (kW)	0.279	0.279	0.279	0.279	0.279	0.279
	Q_d (kVAr)	0.0185	0.0146	0.0123	0.0248	0.0208	0.0181
	V_g (Volt)	418	416	416	420	418	417
18%	V_{gTHD}	3.09	2.97	2.92	6.82	6.78	6.74
	i_{gTHD}	1.30	1.24	1.21	1.83	1.79	1.75
	PF_g	0.98	0.98	0.98	0.98	0.98	0.98
	P_w (kW)	0.279	0.279	0.279	0.279	0.279	0.279
	Q_d (kVAr)	0.0234	0.0195	0.0172	0.0301	0.0261	0.0233
	V_g (Volt)	418	416	416	420	418	417
25%	V_{gTHD}	3.26	3.21	3.19	7.06	6.97	6.92
	i_{gTHD}	1.79	1.67	1.67	2.0	1.95	1.93
	PF_g	0.98	0.98	0.98	0.98	0.98	0.98
	P_w (kW)	0.279	0.279	0.279	0.279	0.279	0.279
	Q_d (kVAr)	0.0321	0.0282	0.0259	0.0393	0.0353	0.0325
	V_g (Volt)	416	415	415	416	415	415
30%	V_{gTHD}	3.49	3.41	3.39	7.23	7.02	6.98
	i_{gTHD}	1.97	1.89	1.83	2.11	2.03	1.97
	i_{wTHD}	1.87	1.82	1.78	3.04	3.00	2.97
	PF_g	0.98	0.98	0.98	0.98	0.98	0.98
	P_w (kW)	0.279	0.279	0.279	0.279	0.279	0.279
	Q_d (kVAr)	0.0469	0.0430	0.0407	0.0533	0.0492	0.0464
	V_g (Volt)	418	416	416	420	418	417

Table 5.7: Performance under synchronization of DFIG with rural grid.

Loading condition	Synchro nization stages	MATLAB Simulation Results (MSR)			Experimental Results (HR)		
		THDVg (%)	THDig (%)	PFg	THDVg (%)	THDig (%)	PFg
Load-1	Weak grid	12.67	6.95	>0.7	13.53	7.85	>0.7
	Transition	11.9	3.94	>0.7	12.89	4.89	>0.7
	Stable	7.2	1.07	0.96	8.12	1.87	0.94
Load-2	Weak grid	14.3	7.24				
	Transition	14.7	4.3				
	Stable	8.07	1.61	0.89			
Load-3	Weak grid	18.69	12.72				
	Transition	22.68	11.77				
	Stable	13.1	5.74	0.83			
Load-4	Weak grid	22.12	16.94				
	Transition	28.92	27.97				
	Stable	15.74	9.11	0.58			

ADALINE-LMS and ALMF algorithms. The WE source and DSTATCOM are connected at 1-second and found that <0.9-s is needed for maintaining soft synchronization. Table 5.7 shows the PQ analysis under the synchronization of DFIG with the rural grid. The observed weak grid, transient (transition) and steady-state (stable) stages voltage and current harmonics are 13.53%, 12.89%, 8.12% and 7.85%, 4.89%, 1.87%, respectively.

The algorithm's performance has also been tested for different compositions loads by varying

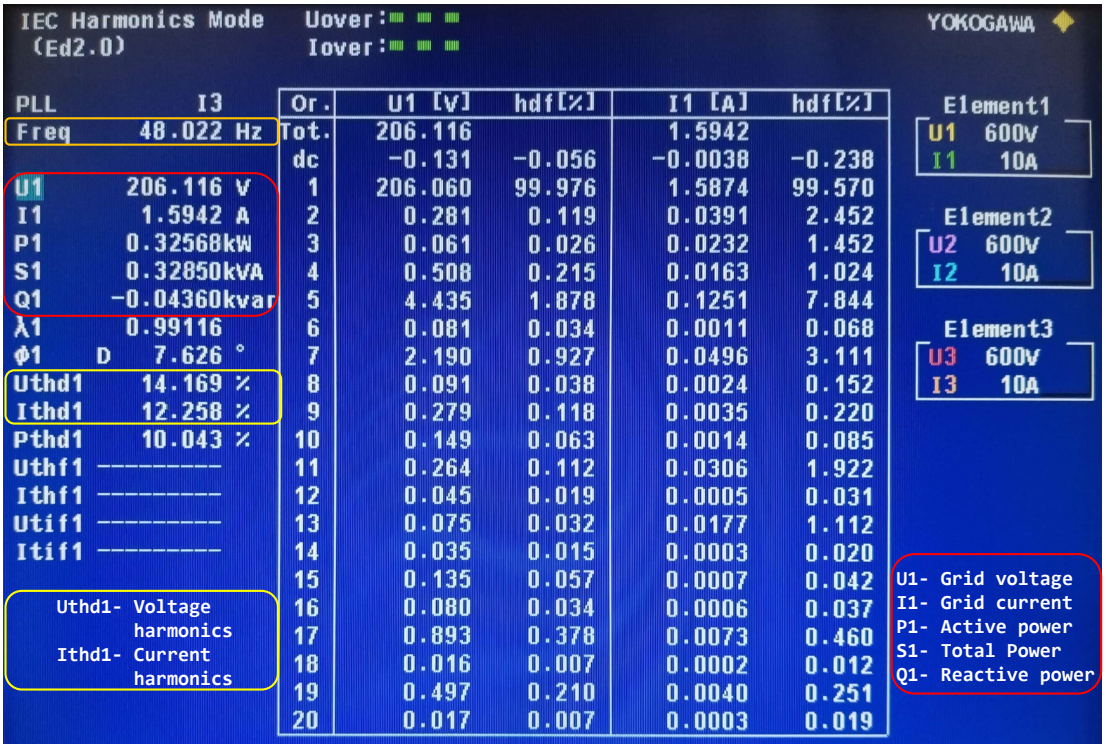

(a)

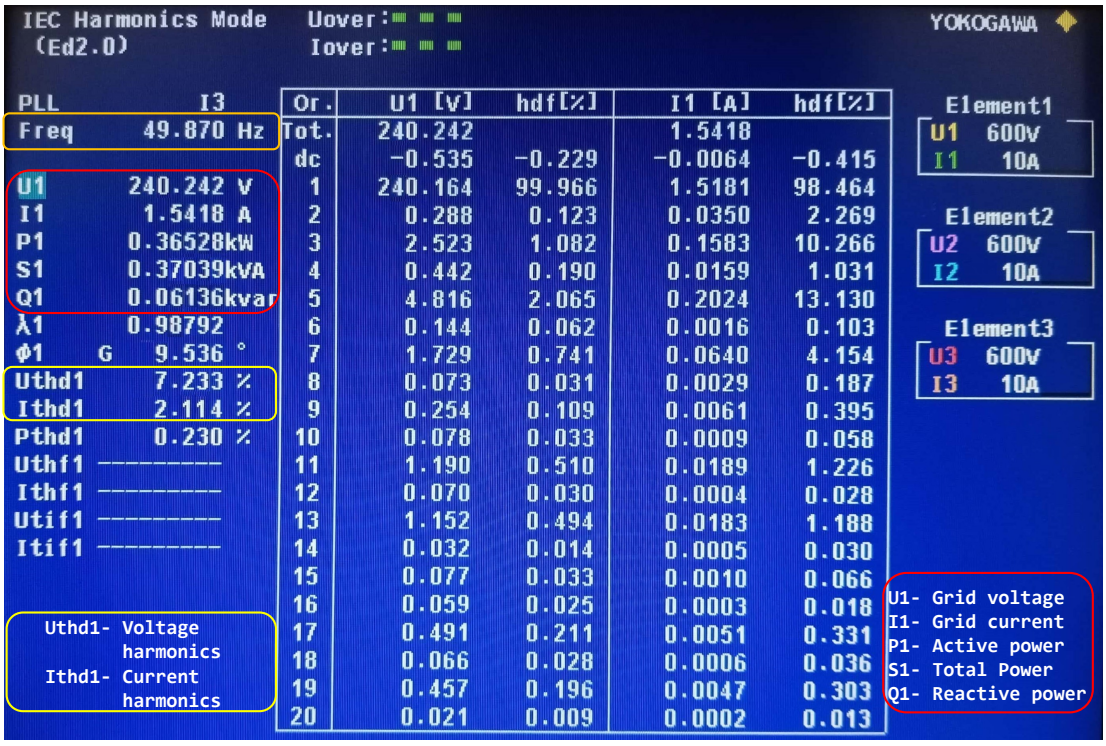

(b)

Figure 5.14: Harmonics and power flow analysis (A) Without DSTATCOM, (b) With DSTATCOM.

the percentage of NL loads (i.e. Load-1=40%, Load-2=50%, Load-3=75% and Load-4=100% NL loads). The harmonics analysis of both simulation and Experimental results are presented in Table 5.7. The results reveal that there is a trade-off between the soft synchronization of DFIG with a high wind penetration level (30%) and the NL loads (beyond 40%). Therefore, such a situation is more challenging and strongly requires more focus.

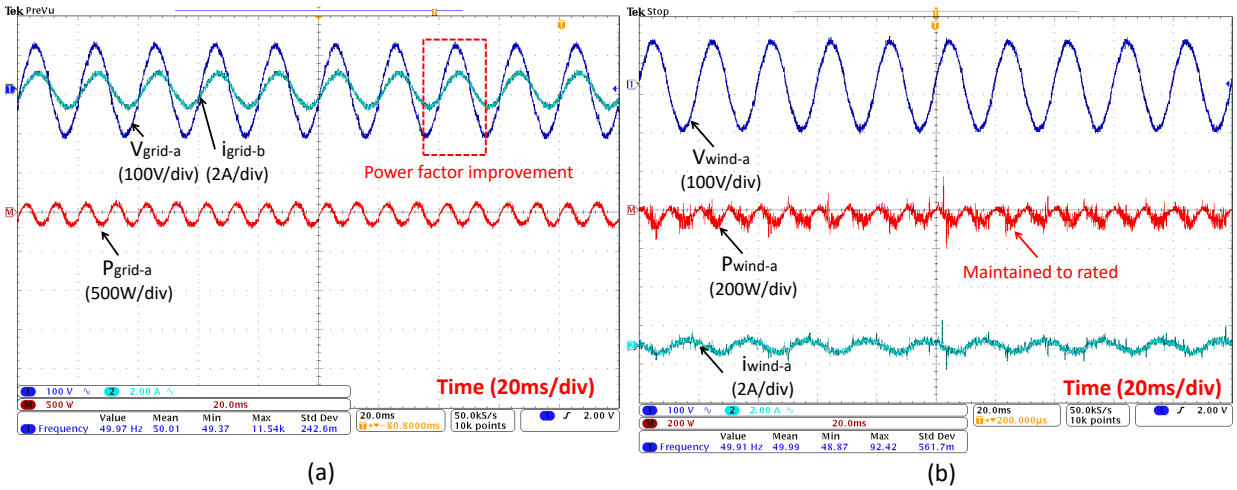

Figure 5.15: Per-phase power analysis (a) Grid and (b) WE source.

5.7 HARMONICS AND POWER FLOW ANALYSIS

Figure 5.14 (a) presents the harmonics and power analysis of the system without DSTATCOM. The observed current and voltage harmonics are 12.258% and 14.169%, respectively. The active and reactive powers seen at PCC are 0.32568 kW/phase and -0.04360 kVAr/phase, respectively. The observed voltage at PCC is 206.116 V. These results do not follow the international PQ standards.

The harmonics and power analysis with the DSTATCOM are present in Fig. 5.14 (b). The observed current and voltage harmonics are 2.114% and 7.223%, respectively. The observed voltage at PCC is 240.242 V. The obtained results are well under the allowed levels of PQ standards. PCC's active and reactive powers are 0.3652 kW/phase and 0.06136 kVAr/phase, respectively. These results show that the DSTATCOM injected the optimized required reactive power (0.01776 kVAR/phase) at the PCC to maintain the grid voltage stability, harmonics and allow a high 30% WE penetration level. Fig 5.15 (a) (b) shows the grid and wind power analysis. The grid is delivered the 0.2722 kW/phase (i.e. 0.816 kW) power at the PCC. The WE source is delivered the 0.093 kW/phase (i.e. 0.279 kW) power with the rated capacity of 0.400 kW.

5.8 COMPARATIVE ANALYSIS

Figure 5.16 presents the comparative analysis of the proposed delayed least mean fourth control algorithm with the algorithms based on Synchronous Reference Frame (SRFT), Adaptive Linear Neural Network-Least Mean Square (ADALINE-LMS) and Adaptive Least Mean Fourth (LMF). It can be observed that the dc-link voltage of DSTATCOM is maintained to reference value with fewer fluctuations using the proposed adaptive algorithm. Table 5.8 presents the comparison of various algorithms used to enhance WE penetration and the proposed algorithm. It can be observed that the DLMF algorithm is superior in terms of voltage stability, accuracy, harmonics minimization and reduction in DSTATCOM size compared with algorithms published in the literature.

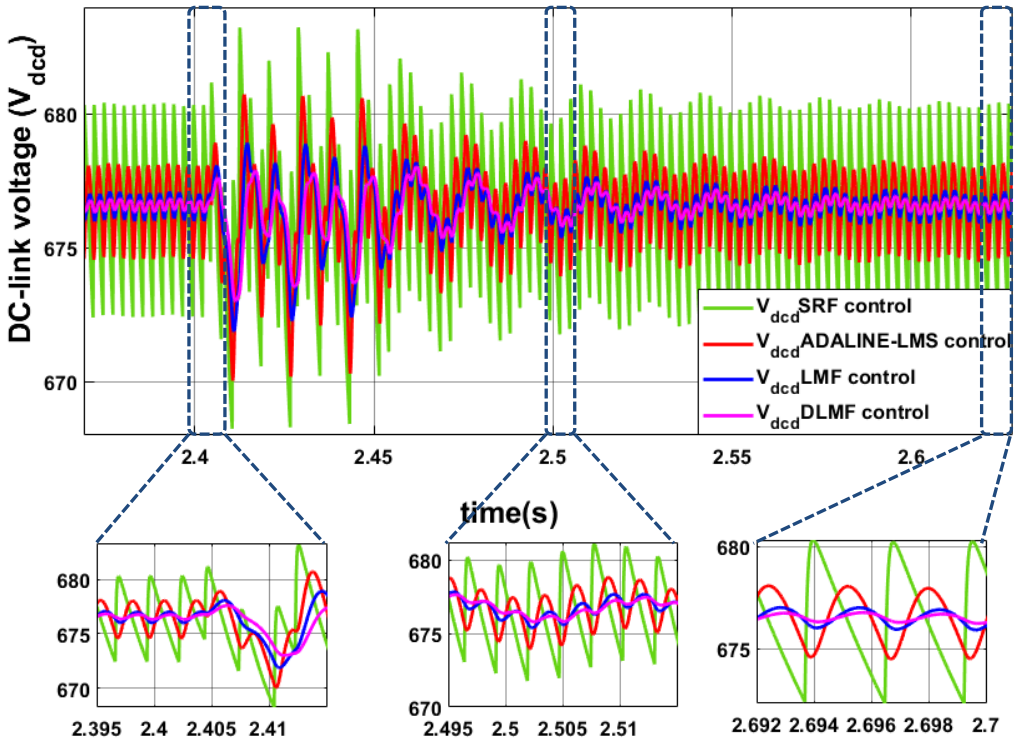

Figure 5.16: DC-link voltage based comparison analysis.

Table 5.8: Comparative analysis.

Attributes	Without DSTATCOM	DSTATCOM with SRFT	DSTATCOM with ADALINE-LMS	DSTATCOM with ALMF	DSTATCOM with DLMF
Nature	-	PLL based	Adaptive	Adaptive	Adaptive
Computational burden	-	High	Low	Low	Moderate
Accuracy of power estimation	Weak	Good	Excellent	Excellent	Excellent
Accuracy in voltage tacking	Weak	Moderate	Excellent	Excellent	Excellent
Accuracy in wind speed variations	Weak	Moderate	Excellent	Excellent	Excellent
Voltage harmonics mitigation	13.22%	8.9%	7.89	7.46%	7.23%
Current harmonics mitigation	12.23%	3.95%	2.41	1.52%	2.11%
Power Factor	Low	Moderate	Ascending tendency	Near to unity	Near to unity
DC-link voltage of DSTATCOM	-	680 V with high oscillations	680 V with fewer oscillations	680 V with fewer oscillations	680 V
DC-link voltage of built-in converter	1150 V	1150 V	1150 V	1150 V	1150 V
Sampling time (Experimental)	-	50 μ sec	30 μ sec	30 μ sec	40 μ sec
Sampling time (Simulation)	-	5 μ sec	5 μ sec	5 μ sec	5 μ sec
WE penetration	Less than 20%	20%	25%	25%	30%
Reduction in DSTATCOM rating	-	30-50%	Up to 70%	Up to 80%	Up to 85%

5.9 CONCLUSIONS

The Delayed-LMF algorithm controlled DSTATCOM method is successfully implemented for improving WE penetration levels (up to 30%) into the grid SCR 2.74 with the proliferation of various loads. The proposed method resolved the emerging challenges related to the high WE penetration into the rural grid under the rated and minimum wind-speed dynamics. The DC-link voltage of the DSTATCOM is maintained at reference voltage under the various strength of the grid with a significantly less reactive power margin. Proposed DLMF optimizes DSTATCOM reactive power injection, thereby reducing the size by 85%. The smooth synchronization is also achieved within 0.9 seconds. The simulation and experimental results reveal that the grid PF, harmonics, load perturbation and voltage stability align with the range described by the international IEEE 519-2014 and EN-50160 standards. Thus, current technical research efforts help rural peoples take the benefits of clean and green energy.